An ab Initio Periodic Study of NiO Supported at the Pd(100) Surface. Part 1: The Perfect Epitaxial Monolayer

Anna Maria Ferrari* and Cesare Pisani

Dipartimento di Chimica IFM and Centre of Excellence NIS (Nanostructured Interfaces and Surfaces), Università di Torino, via Giuria 5, 10125 Torino, Italy

Received: December 20, 2005; In Final Form: February 22, 2006

The epitaxial monolayer of NiO on Pd(100) has been theoretically simulated using a hybrid-exchange GGA-DFT Hamiltonian and a slab model, periodic in two dimensions. This "perfect" system is an essential reference for the simulation of nonstoichiometric two-dimensional phases which are formed during the deposition of nickel on palladium in the presence of oxygen. The adequacy of the computational procedure is discussed, especially as concerns the use of a thermal smearing technique which has been adopted to improve the convergence properties of the SCF procedure and to prevent the onset of nonphysical spin-polarized solutions. The equilibrium configuration corresponds to antiferromagnetic order in the overlayer, with oxygens on top of the surface Pd atoms; the ad-film is slightly corrugated with Ni closer to the surface by 0.1 Å with respect to O. The interaction energy is quite small, 0.20 eV/NiO unit (about 5 kcal mol^{-1}); correspondingly, the electronic and magnetic properties of the Pd slab and the isolated NiO monolayer are only marginally affected by the interaction.

1. Introduction

Thin epitaxial oxide films on metals have been the object of numerous studies in recent years.[1−3] The continuous improvement of experimental techniques, both as concerns the preparation of the samples and their characterization, allows unique features of such two-dimensional (2D) phases to be discovered and new and unexpected structures to be identified. Apart from the relevance of those studies for the basic understanding of metal−oxide interfaces, these systems are interesting for their prospective importance in nanotechnological applications (electronic or magnetic devices, nanocatalysts, and so on).[4] The NiO/Pd(100) system provides a beautiful example of the wide variety of 2D structures of a single metal−oxide interface which can be formed in a controlled way. In a recent series of papers, Granozzi, Netzer, and co-workers have provided a detailed description of the evolution of that system with increasing NiO coverage, depending on the mode of preparation.[5−8] In most of their experiments, the oxide overlayer is grown via a reactive deposition procedure, by dosing Ni at room temperature in the presence of an oxygen background and by performing cycles of annealing at higher temperatures. In particular, they have succeeded in setting up a well-defined procedure whereby to realize an oxide monolayer, fully wetting the surface, with an almost perfect c(4 × 2) 2D structure. Through a combination of different experimental techniques (LEED, XPS, XPD, and STM), the new phase has been identified as an epilayer of monoatomic thickness with Ni_3O_4 stoichiometry,[6,7] characterized by a rhombic regular distribution of Ni vacancies. On the contrary, the simple epitaxial monolayer of stoichiometric nickel oxide (hereafter referred to as NiO-ML) is never identifiable with certainty in the STM images. An attempt to explain this puzzling evidence has been provided in a joint paper by the main researchers of the two experimental groups just mentioned and by the present authors:[9] new STM images were provided and the results of theoretical calculations were presented, both supporting the hypothesis that the c(4 × 2) phase is growing through a 2D reaction between nanoclusters of quasi-stoichiometric nickel oxide and a preexisting regular (2 × 2) O/Pd phase.

This is an example of how computer simulations can be helpful in this area of research to validate or reject structure and growth models, to provide data suitable for comparison with the experiment, and perhaps to help experimentalists in the setting up of optimal preparation procedures. As a matter of fact, due to the ever-increasing power of computer codes for 2D periodic structures, their use is spreading for the description of oxide−metal or oxygen−metal interfaces.[10−14] However, the accuracy of the results may be critically dependent on the procedure adopted. In our joint experimental-theoretical paper,[9] the computational technique and the results of the calculations were described summarily for the sake of brevity. In fact, the simulation of the NiO/Pd interface requires closer analysis, not only for better justifying the results presented there but also because it presents a lot of interesting features which are partly common and partly peculiar with respect to other surface-science applications. Two of them are given special attention in the following:

(i) A characteristic feature of the present 2D system is its mixed character, a nonmagnetic conductor supporting a thin *magnetic* insulator. This is a challenge for standard periodic codes usually based on density functional theory (DFT) Hamiltonians. As shown in the following, a hybrid-exchange technique must be adopted to provide a balanced spin-polarized description of the compound system.

(ii) The presence of the metallic substrate makes the system a conductor. This is always a complication, because of the presence of a Fermi surface. In the present case, the 4d Pd bands lie almost entirely below the Fermi level (ϵ_F) but quite close to it, and the density of state (DOS) near ϵ_F may change

* To whom correspondence should be addressed. Tel: +39-011-6707563. Fax: +39-011-6707855. E-mail: anna.ferrari@unito.it.

10.1021/jp057401r CCC: $30.25
Published on Web 03/25/2006

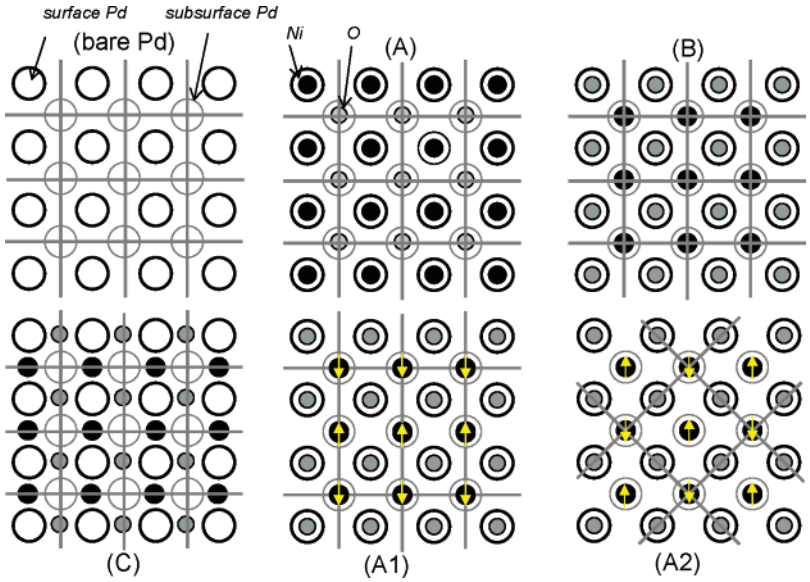

Figure 1. 2D structures considered: the bare Pd(100) slab; epitaxial, ferromagnetic NiO-ML/Pd in the three high-symmetry configurations (A, B, and C); the two most stable antiferromagnetic phases of (B) NiO-ML/Pd. The symbols of the atoms are indicated. The 2D unit cell is shown in all cases.

dramatically with the type of interface. Furthermore, the conducting character makes convergence of the self-consistent-field (SCF) procedure very difficult. To alleviate these problems, a *smearing* procedure is often adopted, which consists of assigning a fractional occupancy to one-electron states in a proximity of ϵ_F, owing to a Fermi−Dirac finite-temperature distribution. The consequences of this procedure, which is adopted also in the present case, deserve critical attention.

These questions and related ones are addressed in the present work with reference to the simulation of the bare Pd(001) surface and of the same covered with epitaxial NiO-ML. The particularly simple character of these two phases will allow us to explore in detail the different topics. The computational setup selected on the basis of the present analysis will be used, in a subsequent paper,[15] to describe the structural, magnetic, electronic, and energetic properties of c(4 × 2) and of (2 × 2) O/Pd, the two phases being related to each other according to the hypothesized mechanism of surface reaction.[9] All the present calculations have been performed by adopting a periodic slab model and DFT Hamiltonians as implemented in CRYSTAL,[16] a periodic code which adopts as a basis set Gaussian type functions (GTFs), at variance with most programs for solid-state and surface-science applications which use plane waves (PWs) instead. A very attractive peculiarity of CRYSTAL is that it may treat the nonlocal exchange operator of the Fock Hamiltonian and is therefore ideally suited for exploring the effectiveness of hybrid-exchange functionals in a periodic context. Among the numerous applications,[17] the recent studies of MgO/Ag[10] and NiO/Ag[10,11] can be mentioned for their relevance in the subsequent discussion.

The structure of this paper is as follows. Section 2 presents the techniques adopted, with identification of the computational parameters and variables to be tested. The results are presented and discussed in section 3. Section 3.1 concerns the study of the substrate. Starting from the known properties of bulk palladium, a model for the slab is selected as a compromise between accuracy, flexibility, and feasibility. This analysis involves the choice of slab thickness and basis set and the study of the effect of the fraction α of exact exchange and of the value β of the smearing parameter on the quality of the solution; it is shown in particular that, for a certain range of α and β values, palladium exhibits a spontaneous (and unphysical) spin polarization. The properties of the isolated NiO-ML are briefly reviewed in section 3.2, while the compound system NiO-ML/Pd(100) is treated in section 3.3 with reference to the two isolated subsystems. The effect of the interaction on the electronic and magnetic characteristics of the two moieties is analyzed and discussed in section 3.3.

2. Computational Details

2.1. Geometry. As is customary in this kind of simulation, the semi-infinite Pd(100) surface, either bare or covered by NiO, has been modeled with a slab of finite thickness. The use of GTFs as basis functions allows CRYSTAL to treat the system as a *single* slab, rather than as a 3D stack of slabs separated by vacuum regions, as it is required when PWs are used as a basis set. The critical issue of the slab thickness is discussed in section 3.1, taking as a reference the known properties of Pd bulk. While it was found that slabs of five Pd layers can provide a satisfactory description of the most important surface properties, the performance of a three-layer Pd slab has also been tested and found to be an acceptable model in most respects. The latter simplified model was used systematically to reduce computational costs, and only for a limited number of cases the results were checked for validation against those obtained with the thicker slab. The 2D cell parameter of the slab has been taken throughout to coincide with that obtained from the optimization of bulk Pd, and it defines the value of the cell parameter of epitaxial oxide. This constraint may introduce stresses in the overlayer, due to the mismatch between the two separated moieties; in the present case, this effect is almost negligible because the lattice parameter of the *isolated* NiO-ML will be shown to practically coincide with that of the substrate. Two-sided adsorption has been considered in all cases. This choice not only increases symmetry and reduces computational costs but also prevents artificial fields to develop across the slab. The plane symmetry and the unit 2D cell of the compound system depend both on the configuration of the overlayer and on its magnetic structure. The cases considered in the present work and the nomenclature adopted are shown in Figure 1. Geometry

optimizations have been carried out using the procedure recently implemented in CRYSTAL; at the present, it requires the numerical calculation of gradients for conductors, since analytical gradients are only available for insulating systems. All O and Ni ions in the adlayers have been allowed to relax whereas the Pd atoms have been kept fixed at their bulk values.

2.2. Hamiltonian. A delicate issue is the choice and calibration of a suitable Hamiltonian, apt at providing a satisfactory description of the properties of the different substructures. Our previous studies have shown that a DFT approach based on the generalized gradient approximation as proposed by Perdew and Wang (the PWGGA exchange-correlation functional)[18] performs satisfactorily for the evaluation of the structural and electronic properties of metallic systems. This is confirmed for the case of Pd, as shown in section 3.1. On the other hand, it is known that standard DFT approaches provide an unsatisfactory description of magnetic insulators such as NiO.[19] As in our previous study of NiO/Ag,[10] a hybrid-exchange Hamiltonian has been adopted here of the type proposed by Becke,[20] where the exchange expression of the PWGGA functional is mixed with a percentage α of the exact Hartree−Fock exchange. Reference has been made to the following semiempirical formula for the exchange-correlation energy[20]

$$E_{XC}^{\text{hybrid,PW}} = (1-\alpha)(E_X^{\text{LSDA}} + \alpha_X E_X^{\text{BECKE}}) + \alpha E_X^{\text{HF}} + (1-\alpha_C)E_C^{\text{LSDA}} + CE_C^{\text{PWGGA}}$$

where LSDA is the local spin density approximation composed of the Dirac−Slater exchange[21] and the Vosko, Vilk, and Nusair correlation functional[22] and HF represents the exact part of the exchange energy. In such a formulation, the last term is the only difference with respect the original Becke proposal which used the LYP correlation functional.[20] The empirical coefficient α, α_X, and α_C have been set to 0.2, 0.9, and 0.81 by Becke; α_X and α_C have been kept unvaried in the present work. The α value has been determined on the basis of test calculations with α ranging from 0 (pure PWGGA) to 0.8 (F80PW, the two figures in the abbreviation indicating the α percentage). A F35PW Hamiltonian has been finally adopted: this choice is validated in sections 3.1, 3.2, and 3.3. It has to be noticed that, while bare Pd could be studied with a spin-restricted (SR) Hamiltonian, the same is not true for the compound system, due to the intrinsically magnetic character of NiO. It turns out that even bare Pd turns out to be magnetic if treated with a spin-unrestricted (SU) technique, for certain values of the exchange percentage α and of the smearing parameter β (see below). This puzzling problem is discussed in section 3.

2.3. Smearing. The SU hybrid-exchange calculations reported in the next sections are computationally very demanding and not only because of the size of the unit cell. In most cases, the calculation concerns a conducting, heterogeneous, magnetic system, with a high density of electron states near the Fermi level ϵ_F. The modification of the *two* Fermi surfaces (those of α and β electrons) along the SCF procedure is a source of instabilities and convergence difficulties and requires a careful setting of the computational parameters. To make the procedure less sensitive to the position of ϵ_F and to the density of the sampling *k* net, a smearing technique has been proposed since long[23,24] and is embodied in the CRYSTAL program.

Essentially, it consists of attributing to each one-electron state $\psi_i(k)$ with eigenvalue $\epsilon_i(k)$ a fractional occupancy f_i to be used in the reconstruction of the density matrix, owing to a Fermi−Dirac distribution function, characterized by a *smearing parameter* β that corresponds to a *smearing temperature* $T_S = \beta/k_B$

$$f_i(k;\beta) = \left[1 + \exp\left(\frac{\epsilon_i(k) - \epsilon_F}{\beta}\right)\right]^{-1}$$

The DF theory at the finite-temperature T_S is derived[23] as a generalization of the Hohenberg and Kohn theorem,[25] by minimizing with respect to $\rho(r,T_S)$ the free energy of the system, $F(T_S) = E(T_S) - T_S S(T_S)$, with both the internal energy *E* and the configurational electron entropy *S* depending on the occupation numbers, hence on T_S.

The use of this finite-temperature scheme is merely a device whose purpose is to smooth discontinuities at the Fermi level. The required quantity is the ground-state zero temperature energy, E_0. With reference to the theory of the free-electron gas, it is easily shown that for small *T* values the free energy deviates from E_0 by a quantity quadratic in *T*, $F(T) = E_0 - 1/2\gamma T^2$, and that the deviation of the internal energy is equal and opposite, $E(T) = E_0 + 1/2\gamma T^2$.[26−28] The best estimate of E_0 for *T* approaching zero is therefore, $(F(T) + E(T))/2$, whose deviation from E_0 is only $O(T^3)$. In sections 3.1 and 3.3, it is verified whether this approximation is still accurate enough in the present cases where the system exhibits a behavior very different from that of the free-electron gas even in proximity of ϵ_F. While very effective, this technique may cause appreciable effects both on energy and on electronic structure data, for instance, spin polarization. Reaching convergence for very small β values was anyhow very difficult, and our best estimates were obtained by extrapolating to zero results obtained with β ranging from 0.005 to 0.04 hartree.

2.4. Basis Set and Pseudopotentials. The choice of a basis set (BS) of GTFs is known to be another critical issue in applications such as the present one where interactions have to be described involving tiny energy differences: very extended sets cannot be adopted both because computational times increase very rapidly and because problems arise of quasi-linear dependence with increasing BS size. The BS adopted for the NiO overlayer is the same as calibrated in our previous study of that species interacting with Ag(100):[10] it consists of all-electron 8-411G functions for the O^{2-} ion and in the Hay−Wadt small core pseudopotential[29] together with 3sp/2d contracted GTFs for Ni^{2+}. As concerns Pd, two different BSs have been tested. The larger one (hereafter referred as the L-basis) is of the same quality as that used to describe the silver support in our previous works[10−12] and consists of a "Stuttgart" small core relativistic pseudopotential[30] with 4s/4p/2d GTFs to describe the valence electrons; the smaller one (S-basis) consists of a Hay−Wadt small core pseudopotential[29] together with 4sp/2d to describe the outer electrons. Essentially, the L-basis was optimized for the atom and then slightly modified for solids, while the S-basis was optimized for bulk Pd. Further details are found in the CRYSTAL database.[31j] The number of electrons explicitly considered is 18 for Pd and 18 for Ni (corresponding to the electron configurations $4s^25s^24p^64d^{10}$ and $3s^24s^23p^63d$,[8] respectively). All energy data reported in this work have been corrected for the basis set superposition error (BSSE) by applying the standard counterpoise method.[32]

3. Results

3.1. Pd Bulk and Slab. A preliminary study has been performed on Pd bulk for checking the adequacy and limitations of the computational setup. As discussed in the previous section, a number of combinations have been tried, involving the

TABLE 1: Calculated vs Experimental Data for Pd Bulk

	PWGGA[a]		PWF35[a]		
	S-basis[a]	L-basis[a]	S-basis	L-basis	experiment
a (Å)[b]	3.95	3.96	3.93	3.93	3.89
B (Mbar)[b]	1.83	1.69	1.81	1.96	1.80
E_{coh} (eV)[b]	5.20	4.19	3.32	2.50	4.10
$\epsilon_m(k)$ (eV)					
$\Gamma_{2,3,4}$	−2.86	−2.78	−3.81	−3.75	-2.55 ± 0.15
$\Gamma_{5,6}$	−1.33	−1.31	−2.18	−2.18	-1.15 ± 0.1
$\Gamma_{2,3}$	−2.90	−2.82	−4.03	−4.00	-2.4 ± 0.2
L_7	5.63	5.80	9.93	9.99	7.77 ± 0.3

[a] For the definition of the two Hamiltonians (PWGGA and F35PW) and of the two basis sets (S-basis and L-basis), see text; in all cases, the smearing parameter β was set at 0.01 Ha and a spin-restricted (SR) calculation was performed. [b] a is the lattice constant, B the bulk modulus, and E_{coh} the cohesion energy with respect to isolated atoms. The experimental values of B and E_{coh} are from the database;[34] those concerning the position of a few valence and conduction bands with respect to the Fermi level at two special k points are from ref 34.

percentage of exact exchange in the DFT Hamiltonian, the use of a richer (L-basis) or a poorer (S-basis) BS, the effect of the smearing parameter, and the use of an SR or SU approach. Table 1 reports some structural, elastic, energetic, and band-structure data calculated for bulk Pd with the two basis sets and with pure DFT (PWGGA), or 35% of Hartree−Fock exchange (F35PW), and compares them to the experimental values.[34] The lattice parameter, $a = 3.93$ Å, differs by only 1% with respect the experimental value, $a = 3.89$ Å, and the bulk modulus is satisfactorily reproduced; cohesive energy is more sensitive to the basis adopted, probably because of the different strategy adopted for their selection. Bandwidths are in fair agreement with the experiment, although somewhat too expanded when the hybrid Hamiltonian is used; the calculated Fermi surface reproduces very well in all cases the experimental one (see Figure 1 of the Supporting Information). The combination F35PW/S-basis performs reasonably well in all respects and is the one which we finally adopted.

Owing to a Mulliken analysis, the electron configuration may be described as $5sp^{0.99}4d^{9.01}$, indicating that a 5sp−4d hybridization justifies the metallic character of Pd. All the calculations just reported have been performed by imposing perfect spin pairing. As illustrated in Table 2, when this constraint is removed (as it is necessary for describing the interaction with magnetic overlayers) and the HF exchange percentage α in the DFT functional becomes appreciable, a spin-polarized ground-state configuration may become energetically favored. This is to be attributed partly to the fact that Pd is easily magnetizable (its magnetic susceptibility is 567.4×10^{-6} cgs units/mol, while, for instance, it is -19.5×10^{-6} cgs units/mol for Ag) and partly to the fact that the HF exact exchange favors excessively spin-polarized structures, contrary to what happens with pure DFT. As expected, such artificial polarization is partly recovered by increasing the smearing parameter. In fact, for each value of α, there appears to be a critical value of β beyond which the SR solution becomes more stable. This is not the only effect of the smearing technique on the bonding properties: as shown in Table 2, the cohesive energy slightly increases with increasing β, indicating that the correction discussed in section 2.3 is not totally adequate. The influence of α is by far more important; as expected, pure DFT slightly overestimates and HF underestimates the binding energy, with the value $\alpha = 35$ being the best compromise in the present case.

The same Hamiltonian/BS combinations have been considered for exploring the structural, energetic, and electronic properties of the bare Pd(001) surface and their dependence on slab

TABLE 2: Effect of the α and β Parameters on the Results of SU, S-basis Calculations on Pd Bulk

α (%)[a]	β (Ha)[a]	E_{coh}, ΔE_{pol} (eV)[b]	μ (au)[b]
0	0.01	5.18, 0.00	0.00
	0.02	5.27, 0.00	0.00
	0.03	5.35, 0.00	0.00
	0.05	5.57, 0.00	0.00
15	0.01	4.16, 0.10	0.23
	0.02	4.22, 0.00	0.00
	0.03	4.39, 0.00	0.00
	0.05	4.44, 0.00	0.00
25	0.01	3.72, 0.06	0.41
	0.02	3.78, 0.00	0.00
	0.03	3.83, 0.00	0.00
	0.05	3.95, 0.00	0.00
35	0.01	3.30, 0.10	0.44
	0.02	3.35, 0.02	0.24
	0.03	3.40, 0.00	0.00
	0.05	3.43, 0.00	0.00
50	0.01	2.65, 0.13	0.44
	0.02	2.69, 0.10	0.40
	0.03	2.72, 0.00	0.00
	0.05	2.77, 0.00	0.00
80	0.01	1.54, 0.11	0.62
	0.02	1.62, 0.14	0.36
	0.03	1.64, 0.10	0.33
	0.05	1.61, 0.04	0.00

[a] α is the percentage of exact exchange in the DFT Hamiltonian, $\alpha = 0$ corresponding to pure PWGGA, and $\alpha = 35$ to F35PW; β is the smearing parameter. [b] E_{coh} and ΔE_{pol} are the cohesion energy per atom and its gain with respect to the corresponding SR calculation, respectively; μ is the spin Mulliken population.

thickness. Four or five-layer slabs were thick enough to reach convergence in the surface formation energy, amounting to 6.83, 5.49 and 6.57, 4.75 J/m^2 for the four combinations PWGGA/S,L-basis and F35PW/S,L-basis, respectively. Notice, however, that the surface energy computed for the three-layer Pd slab is not far from the corresponding converged value: the surface formation energy obtained with the three-layer model is 6.79, 5.49 and 6.29, 4.75 J/m^2 for the four combinations PWGGA/S,L-basis and F35PW/S,L-basis, respectively. The larger surface energy obtained with S-basis is consistent with the larger value of E_{coh} obtained with that basis set for bulk Pd. No particular structural or electronic features were found to be associated with the formation of the (100) surface. For example, using the F35PW/S-basis combination, the distribution of the Mulliken populations among sp-type and d-type electrons are as follows: for a three-layer slab, 8.814, 9.168 (surface layer), 9.024, 9.010 (central layer); for a five-layer Pd slab, 8.818, 9.166 (surface layer), 9.010, 9.008 (subsurface layer), 8.992, 9.004 (central layer). For comparison, those of bulk Pd are 8.992, 9.008. The slight increase of the d population in surface Pd with respect to bulk Pd is in agreement with literature data.[33] The calculated ϵ_F can be directly associated with the opposite of the experimental work function. The values −3.91, −4.73 eV and −3.84, −4.68 eV computed for the combinations F35PW/S,L-basis with a five-layer Pd slab and a three-layer Pd slab, respectively, indicate a non-negligible dependence on the basis set, even if all results are in reasonable agreement with the experimental value, −5.0 eV.[34] The effect of the slab thickness is less important, and even the band structure does not reveal a significant dependence on this parameter; therefore, to reduce computational costs, most of the simulations described below adopt the three-layer model, with five-layer slabs being used only to check the most important results. All the slab results reported until now are referred to SR calculations. When spin polarization is allowed to occur, it can be alleviated by relatively high β values.

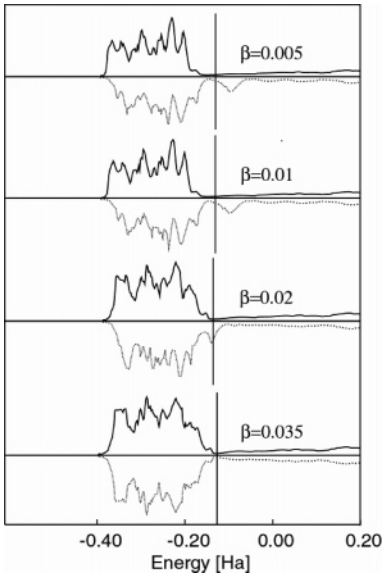

Figure 2. Influence of the smearing parameter β on the density of states (DOSs) for a Pd(100) three-layer slab, as resulting from a F35PW, SU, S-basis calculation. The values of β, in Ha, are reported on each plot. Majority and minority spin DOSs (arbitrary units) are plotted above and below the zero line, respectively. The vertical line in each plot indicates the Fermi level.

The influence of the smearing technique on the electron states close to ϵ_F is illustrated in Figure 2 for a three-layer Pd(100) slab. Minority spin states that were pushed up above ϵ_F become gradually occupied with increasing β, so quenching the artificial spin polarization. Indeed, for the four β values 0.005, 0.01, 0.02, and 0.035 Ha, both the spin population of Pd at the surface (μ = 0.39, 0.37, 0.22, and 0.00) and the spin population in the interior (μ = 0.64, 0.61, 0.26, and 0.00) and the artificial stabilization of the spin-polarized state (ΔE_{spin} = 0.35, 0.18, 0.07, and 0.0 eV/2D cell) gradually vanish, accompanied by a slight upshift of the Fermi level (ϵ_F = −3.91, −3.85, −3.74, and −3.51 eV).

3.2. Isolated NiO Monolayer. The adequacy of the present setup to describe NiO has been discussed in previous work,[12] where the same basis set and the same F35PW Hamiltonian were used and shown to perform quite satisfactorily. With the perfect epitaxy constraint, the antiferromagnetic structure A1, shown in Figure 1, is more stable by only 0.07 eV/NiO unit with respect to FM, while A2 is by 0.09 eV less stable than A1. The nomenclature used to design the antiferromagnetic phases in the NiO monolayer is the same as that reported in ref 35 and differs from that usually employed for bulk NiO (AF1 and AF2) to avoid confusion. This order of stability can be explained in terms of the superexchange interaction mediated by O^{2-} ions between Ni ions of opposite spin.[12] For the sake of reference, we report in Figure 3 the FM, A1, and A2 band structures. They differ considerably, especially as far as the main gap width is concerned: 4.6, 6.1, and 4.8 eV, respectively, to be compared with the calculated value of 5.8 eV for NiO bulk (the experimental bulk value is 4.0 eV). While for each case the calculated width depends critically on the amount of HF exchange in the hybrid functional,[12] the relative value depends on the importance of antibonding interactions between lonely occupied d-type AOs on Ni and p-type AOs on O in the highest occupied crystalline orbital (HOCO); this is in turn dictated by the periodic distribution of the spins and by the *k*-symmetry of the HOCO, as shown schematically in the insets of Figure 3. A similar analysis will help us to understand what happens when a regular pattern of cation vacancies is introduced, as will be

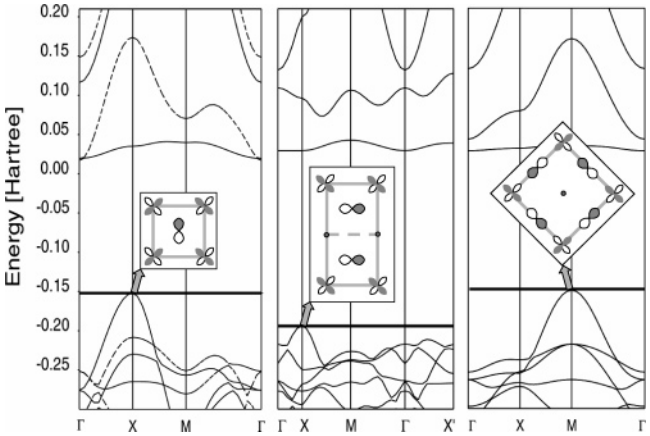

Figure 3. Band structure of the isolated NiO monolayer (i-NiO-ML) in the three magnetic configurations depicted in Figure 1: FM (left), A1 (center), A2 (right). The insets show schematically the structure of the highest occupied crystalline orbital (HOCO) at $k = (1/2, 0)$, $(0, 1/2)$, and $(1/2, 1/2)$ in units of the reciprocal lattice vectors, respectively. The $d_{x^2-y^2}$ orbital which participates in the HOCOs is one of the two singly occupied d-type orbitals on nickel (*x* is the direction of the Ni−O bond), the other being a d_{z^2} orbital which contributes to states of lower energy. In A1 and A2 HOCOs, the dot marks the position of the Ni atom of opposite spin.

discussed at length in the next paper:[15] in fact, the band structure may change dramatically in that case, which has been pointed out by some authors.[36,37] Despite such differences in the band structures, the values of Mulliken electron charges and magnetic moments are similar in the three configurations (FM, A1, and A2, in this order), which justifies the closeness of their energies: $q(Ni) = -q(O) = 1.75, 1.74, 1.76$ au; $\mu(Ni) = 1.84, 1.81, 1.84$ au; $\mu(O) = 0.16; 0; 0$ au. Let us comment finally on the mismatch between NiO and Pd. The calculated misfit between the two bulk structures (corresponding to lattice constants of 4.19 and 3.93 Å) is 6.6% and is close to the experimental value of 7.2% (4.1705 and 3.89 Å). However, i-NiO-ML, the isolated oxide monolayer, exhibits a considerable contraction associated with an energy gain of 0.3 eV/NiO unit: its 2D lattice constant at equilibrium is reduced to 3.91 Å, resulting in practically perfect matching with Pd, within 0.5%. A similar contraction had been observed in the case of i-MgO-ML.[10] Of course, when thick NiO epilayers are formed, considerable strains are produced which must be released somehow; this problem has been discussed for the parallel case of NiO/Ag(001)[11] and is not treated here any further.

3.3. Supported NiO Monolayer. We report below the results of calculations for the NiO-ML/Pd system performed with an SU-F35PW Hamiltonian: the reasons for this choice have been discussed in the previous sections. For computational convenience, the S-basis was adopted for Pd, whose adequacy has been shown to be questionable; nevertheless, we believe that it allows a fairly balanced comparison between results referring to similar magnetic and geometric conformations and permits the effect of computational parameters to be tested.

The data reported in Table 3 are referred to the FM structure of the overlayer, without allowing for its rumpling. They are intended to give a first guess on the different stabilities of the three epitaxial arrangements (A, B, and C) shown in Figure 1 and to test the effect of the smearing parameter and of the slab thickness on electronic structure and energy. First notice that the BSSE correction is practically the same in all cases (≈0.32 eV/NiO unit) and comparatively very important; from now on, we shall refer to the corrected adsorption energies as BE_C. Consider next the effect of the smearing parameter. While its

TABLE 3: Geometric, Electronic, and Energetic Properties of the NiO-ML/Pd Phase, Calculated with the F35PW Hamiltonian for the A, B, and C Configurations (see Figure 1) and with Different Values of Slab Thickness and Smearing Parameter β (Ha)

	A		B				C	
	five-layer; $\beta = 0.01$	three-layer; $\beta = 0.03$	five-layer; $\beta = 0.01$	five-layer; $\beta = 0.03$	three-layer; $\beta = 0.01$	three-layer; $\beta = 0.03$	five-layer; $\beta = 0.01$	three-layer; $\beta = 0.03$
z/Å[a]	2.71	2.68	2.29	2.36	2.37	2.35	2.45	2.44
q (Ni)[b]	1.71	1.73	1.73	1.71	1.74	1.71	1.73	1.72
q (O)[b]	−1.71	−1.69	−1.70	−1.69	−1.72	−1.69	−1.69	−1.67
q (Pd_{surf})[b]	0.03	−0.03	0.00	0.02	−0.02	0.01	0.05	−0.04
μ (Ni)[b]	1.80	1.76	1.79	1.75	1.81	1.75	1.79	1.76
μ (O)[b]	0.13	0.11	0.09	0.13	0.14	0.13	0.14	0.12
μ (Pd_{surf})[b]	0.30	0.02	0.55	0.00	0.01	0.00	0.30	0.02
BE/eV[c]	0.55	0.26	0.73	0.38	0.45	0.39	0.68	0.32
BE_C/eV[c]	0.26	−0.04	0.40	0.088	0.12	0.074	0.38	−0.013
ϵ_F (Δ)/eV[d]	−3.37 (0.54)	−2.69 (0.89)	−1.34 (2.57)	−1.98 (1.59)	−1.77 (2.08)	−1.98 (1.60)	−2.87 (1.04)	−2.44(1.14)

[a] Ferromagnetic (FM) order is assumed. No rumpling of the overlayer is allowed to occur: z is the equilibrium distance between the surface plane of the substrate and the overlayer. [b] Mulliken net charges q and spin populations μ are expressed in atomic units. [c] BE and BE_C are the binding energies per NiO unit before and after the BSSE correction and are calculated with reference to the noninteracting subsystems, the unpolarized Pd slab, and the FM-NiO isolated monolayer. [d] ϵ_F is the Fermi level; its shift Δ with respect to the corresponding value for the isolated Pd slab is reported in parentheses.

TABLE 4: Geometric, Energetic, and Electronic Properties of the Fully Relaxed NiO-ML Phase for the B and C Configurations, by Assuming A1 Magnetic Arrangement, for Two Values of the Smearing Parameter β (Ha)[a]

	B		C	
	$\beta = 0.01$	$\beta = 0.03$	$\beta = 0.01$	$\beta = 0.03$
z (O)/Å[b]	2.364	2.358	2.511	2.483
z (Ni)/Å[b]	2.264	2.260	2.433	2.405
q (Ni)[c]	1.73 (1.74)	1.70	1.72	1.71
q (O)[c]	−1.66 (−1.74)	−1.64	−1.66	−1.64
q (Pd_{surf}); q (Pd_{inner})[c]	−0.07;−0.05 (0.02;−0.03)	−0.06; 0.00 (0.02;−0.04)	−0.08;0.03	−0.07; −0.01
μ (Ni)[c]	±1.78 (±1.81)	±1.74	±1.77	±1.74
μ (Pd_{inner})[c]	±0.01	±0.02	±0.44	±0.03
BE/eV[d]	0.52	0.43	0.52	0.34
BE_C/eV[d]	0.19	0.11	0.22	0.05
ϵ_F/eV	−3.13 (−3.85)[e]	−3.05 (−3.58)	−4.05 (−3.85)	−3.40 (−3.58)

[a] The F35PW Hamiltonian and three-layer Pd slabs are used. [b] z(X) is the equilibrium distance between the surface plane of the substrate and atom X of the overlayer. [c] Mulliken net charges q and spin populations μ are expressed in atomic units. [d] BE values are the binding energies and BE_C the BSSE corrected binding energies per NiO unit with reference to the bare unpolarized Pd slab and the isolated A1-NiO monolayer. Following the discussion in the text, the data in the first column can be considered a rather reliable description of the equilibrium configuration of NiO-ML/Pd(100). [e] Data for the separated subsystems are reported in parentheses.

influence is not very important as concerns the equilibrium distance of the overlayer from the surface and electronic charges on atoms, using $\beta = 0.01$ brings in unphysical magnetic polarization of the Pd substrate and overestimation of binding energies (compare indeed $BE_C = 0.73$ eV for a five-layer Pd slab and $BE_C = 0.45$ eV for a three-layer Pd slab for which a solution was obtained without Pd spin polarization). Similar to the case of bulk Pd (see section 3.1), such polarization disappears with $\beta = 0.03$ and the corresponding results seem more reliable: we shall discuss below this aspect in more detail. Slab thickness appears to play by far a less important role. Comparing now the three-layer, $\beta = 0.03$ results for the three configurations, the following can be noted. As was the case with the parallel cases of MgO-ML/Ag[10] and NiO-ML/Ag,[12] O atoms preferably sit on top of Pd atoms (B), but the interaction energy is very small (0.07 eV/NiO unit), and the other two configurations are even nonbonding, with the bridge (C) arrangement being anyhow preferred over the other high-symmetry one (A). The entity of the interaction is correlated with the proximity of the overlayer to the surface and to the shift upward of the Fermi level.

For a closer analysis, the two more stable configurations (B and C) have been reconsidered by overcoming some obvious limitations of the previous calculations, that is, (i) including full relaxation of the ions in the overlayer, (ii) considering the most stable magnetic arrangement of the oxide film, that is, A1, and (iii) performing a systematic analysis of the effect of β on the interface properties. For these calculations, a three-layer Pd slab was used and a 2×1 elementary cell employed to allow for the magnetic inequivalence of Ni atoms. The most significant results are collected in Table 4. It is easily seen from inspection of Figure 1 that, for B and C configurations with A1 magnetic order of the overlayer, neither O nor surface Pd atoms may exhibit a net magnetic moment for symmetry reasons; the same is not true for subsurface Pd. This prevents to some extent polarization of the substrate even for small values of the smearing parameter. However, for $\beta = 0.01$ and for the C configuration, alternating rows of magnetically polarized Pd atoms ($\mu = \pm 0.44$ au) are obtained; such an artificial spin polarization of the substrate might explain the relatively high interaction energy for this setting of the computational parameters: therefore, the slightly higher stability of configuration C in Table 4 for $\beta = 0.01$ is only apparent due to this unphysical effect. Let us then compare the two $\beta = 0.03$ columns of Table 4. Again, B is more stable than C by a few hundreths of electronvolts per NiO unit; for either configuration, A1-NiO-ML/Pd is more stable than the corresponding FM one by about 0.12 eV/NiO unit, after taking into account that the reference energy of the isolated ML differs by 0.07 eV in the two cases. On the whole, the adsorption energy is very small, and this is reflected in the very small change in the electronic and structural properties of the interacting subsystems. The overlayer is seen

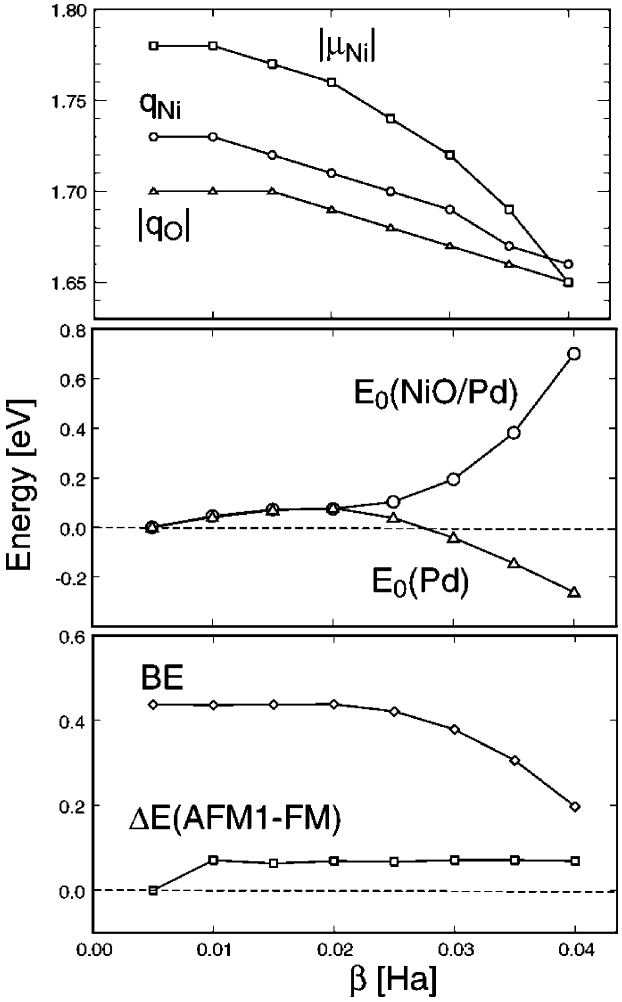

Figure 4. Effect of β on the electronic and energetic properties of NiO-ML/Pd in the B−A1 configuration. Top panel: absolute values of the Mulliken (q) and spin (μ) populations, in atomic units. Central panel: energy per unit 2D cell, E_0, for NiO-ML/Pd (circles) and for the bare, unpolarized Pd slab (triangles), calculated as described in section 2.3. In either case, the zero is set at the corresponding value for $\beta = 0.005$. Bottom panel: binding energy per NiO unit, not corrected for BSSE (BE) and its difference with respect to the corresponding value for the B−FM configuration [ΔE(A1 − FM)].

to possess in all cases a slightly positive net charge, which justifies the slight increase of the Fermi energy with respect to the bare Pd slab.[10] As expected, the rumpling of the overlayer is more important in the B configuration, where Ni atoms above hollow sites come closer to the surface by 0.1 Å than on-top oxygens; the average distance is also smaller in the B with respect to the C configuration and is similar to the corresponding one reported in Table 3 for the FM arrangement. From the present discussion, it may be concluded with some confidence that A1−B is the most stable configuration of an epitaxial NiO monolayer on Pd(100). In the following, we concentrate our attention on this system.

The data reported in Figure 4 allow us to analyze in more detail the effect of β on the calculated electronic and energetic properties of the system and to extrapolate the results to zero smearing temperature; in all those F35PW S-basis calculations, the geometry was kept fixed ($z_O = z_{Ni} = 2.36$ Å). As shown in the top panel of Figure 4, with increasing smearing both the ionicity of the overlayer and the localization of the unpaired electrons on nickel atoms gradually decrease; on the other hand, the total charge on the oxide film (hence the slight transfer of electrons to the metallic substrate) remains almost constant. The central panel shows that for $\beta \leq 0.025$ the energy of the bare and of the oxide-covered slab exhibits the same behavior, which means that in this interval the smearing procedure essentially involves Pd-type electron states: the correction described in section 2.3 appears to be very effective. At higher smearing temperatures, states essentially centered in the oxide may enter the smearing region and the two curves begin to diverge. The consequences are seen in the bottom panel: the BE curve is constant up to $\beta = 0.02$, then begins to decrease, due to the different effect of the smearing procedure on the bare and oxide-covered substrate. It is interesting to analyze the "difference" curve, $\Delta E = \mathrm{BE(A1)} - \mathrm{BE(FM)}$. The effect of the smearing is about the same on the two systems for a wide range of β values, which justifies the approximate constant value, $\Delta E \approx 0.07$ eV. The sharp decrease of ΔE at small β is to be attributed to the fact, already mentioned, that the oxide-covered film exhibits in that case spin polarization in the FM, not in the A1 magnetic arrangement. It can be concluded that, for the A1−B configuration, extrapolation of the calculated data to zero smearing is well justified and that the results obtained for $\beta = 0.01$ are close to that limit. We can then take the data reported in the first column of Table 4 as representative of the equilibrium configuration of NiO-ML/Pd. In particular, the binding energy of the oxide to the metal in its equilibrium configuration can be estimated to be about 0.20 eV/NiO unit with respect to the isolated oxide monolayer in its most stable (A1) configuration. This value can be compared to the energy cost required to prepare an isolated monolayer from bulk crystalline NiO, both in their equilibrium configurations (1.27 eV/NiO unit). It is then clear that the wetting of the Pd surface by the oxide can only take place at very low concentrations of the latter.

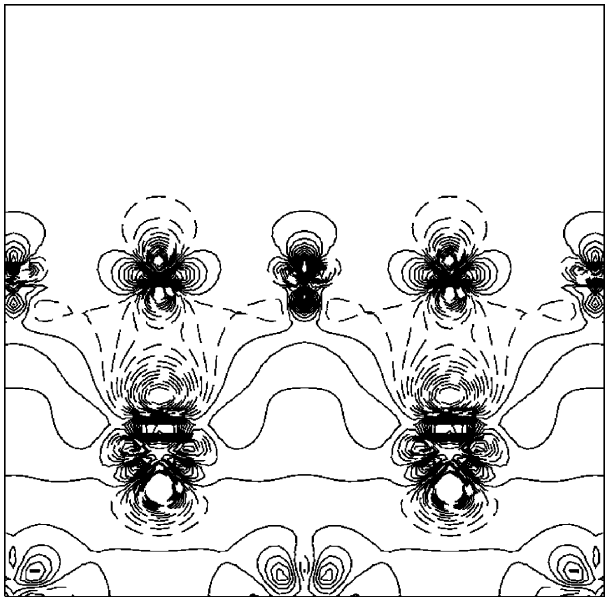

Figure 5. Charge difference density map for the NiO-ML/Pd system in the B−A1 configuration. The plot shows the difference between the electron density for the compound system and the superposition of the electron densities of the two subunits with the same internal geometry. The sections are in a vertical plane through nearest neighbor Ni and O atoms (see Figure 1). Continuous and dashed lines refer to the positive and negative density differences, respectively. The contour lines are drawn at intervals of 0.002 |e|/bohr^3.

The electronic and magnetic features of the equilibrium configuration can now be analyzed with some confidence. All data to be shown and discussed below are referred to the B−A1 configuration, in its rumpled geometry as described in the first column of Table 4, using the value $\beta = 0.01$. The electronic

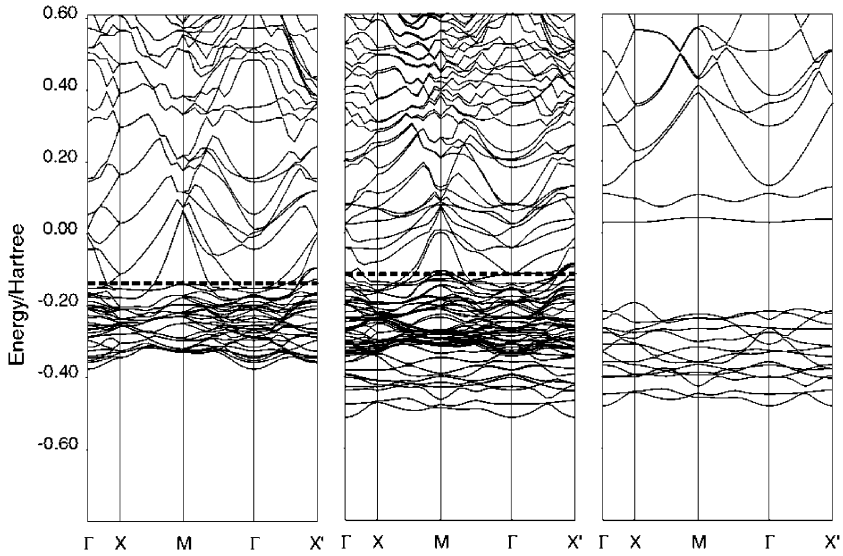

Figure 6. Band structure of the Pd three-layer slab (left), of NiO-ML/Pd(100) in the B−A1 configuration (center), and the A1 isolated NiO monolayer (right). The 2 × 1 2D cell, pertinent to the latter two systems, has been adopted for consistency for the Pd slab as well. The corresponding reciprocal lattice cell is a rectangle centered in Γ with X and X′ at the center of the long and short sides, respectively, and M at a vertex. The dashed line gives the position of the Fermi level.

configuration of the Ni ion in the isolated monolayer $[d_{z^2}^{1.02} d_{xz}^{2.00} d_{yz}^{2.00} d_{xy}^{2.00} d_{x^2-y^2}^{1.18}]$ (x is the direction of the Ni−O bond) does not change significantly upon interaction with the substrate $[d_{z^2}^{1.05} d_{xz}^{1.99} d_{yz}^{1.99} d_{xy}^{1.99} d_{x^2-y^2}^{1.17}]$, which is consistent with the very small binding energy. However, the weak polarization of the composite system, resulting in a slightly positive charge of the overlayer, is evident by inspection of the charge density difference map, Figure 5, which shows that the extra charge of the substrate is mainly located in the interstitial position among surface Pd, in front of the cations of the overlayer and involves a small depopulation (0.06 au) of the 2sp bands of the oxygens in favor of the 5sp orbitals of surface Pd. It affects the Fermi energy that increases by 0.7 eV with respect to that of the bare slab (more than 2 eV without the cation displacement). Indeed, as already reported for NiO/Ag and MgO/Ag,[10,13] the rumpling of the cations has a double favorable effect. From one side, it controls the entity of the charge transfer from the oxide layer to the metal surface, increasing the force of the interaction; on the other side, it reduces the destabilizing effect on the palladium bands by the charged overlayer since the Fermi level upshift is considerably reduced; see Tables 3 and 4. Further information is provided in Figures 6 and 7 which show the band structure and DOS of the NiO/Pd compound, as compared with the corresponding data for the isolated subunits. The band structure confirms the very weak character of the interaction: the bands of the compound are essentially the superposition of those of the constituent subunits, with just a slight upward shift of those of the substrate and a downward shift of those of the overlayer, both due to the minute charge transfer already commented on. Such superposition is evident also in the projected DOSs, the main important difference consisting in a slight decrease of the DOS of the compound system in a strict vicinity of the Fermi level. Also note that the maximum change in the DOSs in the occupied portion of the spectrum takes place around −0.30 Ha, where the band structures of the two subunits exhibit maximum overlap.

The relative stability of the magnetic ordering is not affected by the presence of the metal substrate: indeed, the antiferromagnetic structure A1 is more stable by only 0.070 eV/NiO unit with respect to FM, while A2 is by 0.095 eV less stable than A1. The magnetic coupling constants $J_1 = 5.7$ meV and $J_2 = -20.0$ meV almost coincide with the values computed for the unsupported film ($J_1 = 5.0$ meV and $J_2 = -20.1$ meV). The magnetic coupling constants are computed by means of the Ising spin Hamiltonian: $H = -J_1 \sum_{i,j}{}' S_z^i S_z^j - J_2 \sum_{k,l}{}'' S_z^k S_z^l$, where S_z^i stands for the z component of the total spin on the magnetic center and $\sum'$ and $\sum''$ are extended to the first and second neighbors, respectively (see refs 12 and 19 for details). Such computed values are comparable with those calculated in the case of a NiO monolayer supported at a Ag(100) surface ($J_1 = 3.4$ meV and $J_2 = -31.1$ meV).[12] It is worth noticing that in both cases, NiO-ML/Pd and NiO-ML/Ag, A1 is the preferred magnetic arrangement that is the same of the (100) basal plane of NiO AF2[38] bulk phase being AF2 the favored magnetic order.[39]

4. Conclusions

In the simulation of ultrathin epitaxial overlayers of oxide on metals, the calibration of the computational parameters is often a very delicate issue. Special attention has been devoted here to the problems related to the use of the thermal smearing technique in the study of the interaction of NiO with the (001) face of Pd. It has been shown that such a computational device is very effective both to improve the convergence properties of the SCF procedure and to prevent the onset of nonphysical spin-polarized solutions; however, great care is required to extrapolate the results to zero smearing temperature. In the present case, such an extrapolation has been found to be possible and a rather reliable description has been provided of the epitaxial stoichiometric monolayer of NiO on Pd, from a structural, electronic, magnetic, and energetic viewpoint. The equilibrium configuration has been found to correspond to antiferromagnetic order in the overlayer, with oxygens on top of the surface Pd atoms; the ad-film is slightly corrugated with Ni closer to the surface by 0.1 Å with respect to O. The interaction energy is quite small, 0.20 eV/NiO unit (about 5 kcal mol^{-1}); correspondingly, the electronic and magnetic properties of the two interacting units are only marginally affected. The preferred magnetic arrangement A1 is the same as that reported for NiO-ML/Ag(100). Although NiO-ML/Pd is of no special interest in itself, this "perfect" system is an essential reference for the simulation of

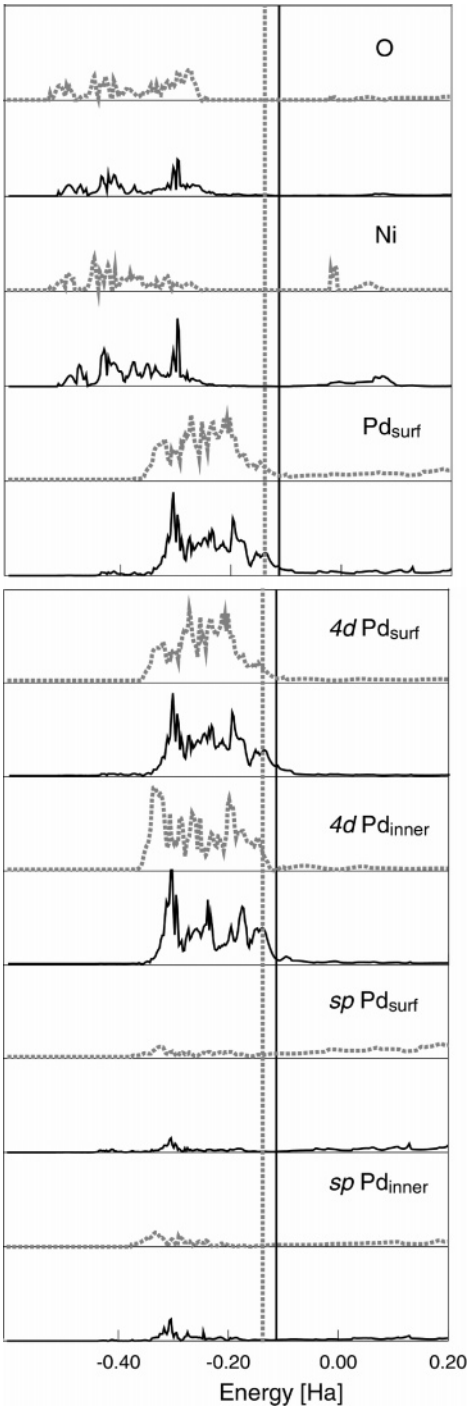

Figure 7. Projected DOSs of NiO/Pd (solid black line) and of the two noninteracing subunits (dashed gray line). The position of the Fermi level is indicated by the vertical lines: solid black for NiO/Pd, dashed gray for the palladium slab. The projections are affected according to a Mulliken population analysis.

nonstoichiometric 2D phases which are formed during the deposition of nickel on palladium in the presence of oxygen and for the bulklike phase observed for thicker film.

Acknowledgment. Useful discussions with Mauro Ferrero and financial support from the Italian Ministry of Instruction, University and Research (MIUR) (program: Difettualità e proprietà catalitiche di film e di cluster superficiali, No. 031153) are gratefully acknowledged. We also acknowledge CINECA for a high-performance computing grant.

Supporting Information Available: Figure showing the palladium Fermi surface taken from an experiment by Vuittelmin.[40] This material is available free of charge via the Internet at http://pubs.acs.org.

References and Notes

(1) Chambers, S. A. *Surf. Sci. Rep.* **2000**, *39*, 105.
(2) Renaud, G. *Surf. Sci. Rep.* **1998**, *32*, 1.
(3) Campbell, C. T. *Surf. Sci. Rep.* **1997**, *27*, 1.
(4) Wollschläger, J.; Viernow, J.; Tegenkamp, C.; Erdös, D.; Schröder, K. M.; Pfnür, H. *Appl. Surf. Sci.* **1999**, *142*, 129.
(5) Sambi, M.; Sensolo, R.; Rizzi, G. A.; Petukhov, M.; Granozzi, G. *Surf. Sci.* **2003**, *537*, 36.
(6) Orzali, T.; Agnoli, S.; Sambi, M.; Granozzi, G. *Surf. Sci.* **2004**, *569*, 105.
(7) Agnoli, S.; Sambi, M.; Granozzi, G.; Atrei, A.; Caffio, M.; Rovida, G. *Surf. Sci.* **2005**, *576*, 1.
(8) Agnoli, S.; Orzali, T.; Sambi, M.; Granozzi, G.; Schoiswohl, J.; Surnev, S.; Netzer, F. P. *J. Electron Spectrosc. Relat. Phenom.* **2005**, *144*−*147*, 465.
(9) Agnoli, S.; Sambi, M.; Granozzi, G.; Schoiswohl, J.; Surnev, S.; Netzer, F. P.; Ferrero, M.; Ferrari, A. M.; Pisani, C. *J. Phys. Chem. B* **2005**, *109*, 17197−17204.
(10) Sgroi, M.; Pisani, C.; Busso, M. *Thin Solid Films* **2001**, *64*, 400.
(11) Lamberti, Groppo, E.; Prestipino, C.; Casassa, S.; Ferrari, A. M.; Pisani, C. *Phys. Rev. Lett.* **2003**, *91*, 046101.
(12) Casassa, S.; Ferrari, A. M.; Busso, M.; Pisani, C. *J. Phys. Chem. B* **2002**, *106*, 12978.
(13) Nokbin, S.; Limtrakul, J.; Hermansson, K. *Surf. Sci.* **2004**, *556*−*558*, 977.
(14) Kokalj, A.; Dal Corso, A.; de Gironcoli, V.; Baroni, S. *Surf. Sci.* **2003**, *191*, 532.
(15) Ferrari, A. M.; Ferrero, M.; Pisani, C., in press.
(16) Saunders, V. R.; Dovesi, R.; Roetti, C.; Orlando, R.; Zicovich-Wilson, C. M.; Harrison, N. M.; Doll, K.; Civalleri, B.; Bush, I. J.; D'Arco, P.; Llunell, M. *CRYSTAL03 User's Manual*; Università di Torino: Torino, Italy, 2003.
(17) Dovesi, R.; Civalleri, B.; Orlando, R.; Roetti, C.; Saunders, V. R. *Rev. Comput. Chem.* **2005**, *1*, 21.
(18) Perdew, J. P. *Electronic structure of solids*; Akademie Verlag: Berlin, 1991.
(19) Moreira, I.; Illas, F.; Martin, R. *Phys. Rev. B* **2002**, *65*, 155102.
(20) Becke, A. D. *J. Chem. Phys.* **1993**, *98*, 5648.
(21) Dirac, P. A. M. *Proc. Cambridge Philos. Soc.* **1930**, *26*, 376.
(22) Vosko, S. H.; Wilk, L.; Nuisar, M. *Can. J. Phys.* **1980**, *58*, 1200.
(23) Mermin, N. D. *Phys. Rev. A* **1965**, *137*, 1441.
(24) Fu, C. L.; Ho, K. M. *Phys. Rev. B* **1983**, *28*, 5480.
(25) Hohenberg, H.; Kohn, W. *Phys. Rev.* **1964**, *136*, B864.
(26) Gillan, M. J. *J. Phys.: Condens. Matter* **1989**, *1*, 689.
(27) Doll, K.; Harrison, N. M. *Phys. Rev. B* **2001**, *63*, 165410.
(28) Kittel, C. *Introduction to Solid State Physics*, 3rd ed.; Wiley: New York, 1968.
(29) Hay, P. J.; Wadt, W. R. *J. Chem. Phys.* **1985**, *82*, 270.
(30) Doll, K.; Pyykkö, P.; Stoll, H. *J. Chem. Phys.* **1998**, *109*, 2339.
(31) www.chimifm.unito.it/teorica/crystal/Basis_Sets.
(32) Boys, S. F.; F. Bernardi, F. *Mol. Phys.* **1970**, *19*, 553.
(33) Sawaya, S.; Goniakowski, J.; Mottet, C.; Saul, A.; Treglia, G. *Phys. Rev. B* **1998**, *56*, 12161.
(34) (a) *CRC Handbook of Chemistry and Physics*, 74th ed.; CRC Press: Boca Raton, FL, 1993. (b) Himpfel, F. J.; Eastman, D. E. *Phys. Rev. B* **1978**, *18*, 5236.
(35) Noguera, C.; Mackrodt, W. C. *J. Phys.: Condens. Matter* **2000**, *12*, 2163.
(36) Elfimov, L. S.; Yunoki, S.; Sawatzky, G. A. *Phys. Rev. Lett.* **2002**, *89*, 216403
(37) Kodderitzch, D.; Hergert, W.; Szotek, Z.; Temmerman, W. M. *Phys. Rev. B* **2003**, *68*, 125114.
(38) Towler, M. D.; Allan, N. L.; Harrison, N. M.; Saunders, V. R.; Mackrodt, W. C.; Aprà, E. *Phys. Rev. B* **1994**, *50*, 5041
(39) Tjemberg, O.; Soderholm, S.; Chiaia G.; Girard, R.; Karlsson, U.; Nylen, H.; Lindau, I. *Phys. Rev. B* **1996**, *54*, 10245.
(40) Vuittelmin, J. J. *Phys. Rev.* **1966**, *144*, 396.